THE ARAUCARIA PROJECT: VLT-FORS SPECTROSCOPY OF BLUE SUPERGIANTS IN NGC 3109—CLASSIFICATIONS, FIRST ABUNDANCES, AND KINEMATICS[1]

C. J. Evans,[2] F. Bresolin,[3] M. A. Urbaneja,[3] G. Pietrzyński,[4,5] W. Gieren,[4] and R.-P. Kudritzki[3]

ABSTRACT

We have obtained multiobject spectroscopy of luminous blue supergiants in NGC 3109, a galaxy at the periphery of the Local Group at $\sim$1.3 Mpc. We present a detailed catalog including finding charts, V and I magnitudes, spectral classifications, and stellar radial velocities. The radial velocities are seen to trace the rotation curves obtained from studies of the H I gas. From quantitative analysis of eight B-type supergiants we find a mean oxygen abundance of $12 + \log{(O/H)} = 7.76 \pm 0.07$ (1 σ systematic uncertainty), with a median result of 7.8. Given its distance, we highlight NGC 3109 as the ideal example of a low-metallicity, dark-matter–dominated dwarf galaxy for observations with the next generation of ground-based extremely large telescopes.

Subject headings: galaxies: individual (DDO 236, NGC 3109) — galaxies: stellar content — stars: early-type — stars: fundamental parameters

1. INTRODUCTION

NGC 3109 is a Magellanic-like spiral galaxy of type SBm (de Vaucouleurs et al. 1991) at the outer edge of the Local Group, at a distance of 1.3 Mpc (Capaccioli et al. 1992; Lee 1993; Soszyński et al. 2006). Its relative proximity and low foreground reddening (Burstein & Heiles 1984) make it well suited to exploring galaxy formation and evolution in dwarf irregulars beyond the Magellanic Clouds.

Photometric studies have suggested that the main body of NGC 3109 has a low, SMC-like metal abundance (Elias & Frogel 1985; Greggio et al. 1993). Moreover, from deep imaging, Greggio et al. noted subtly different populations across the disk of the galaxy that they ascribed to different metallicities/star formation histories in their target fields, to differential reddening, or a combination of both. The galaxy is thought to have a very metal-poor stellar halo (Minniti et al. 1999), although Demers et al. (2003) have argued that the minor axis star counts can be explained by the inclination of the disk, rather than requiring a significant halo population. There also appears to be evidence of interaction with the Antlia dwarf galaxy $\sim$1 Gyr ago (Barnes & de Blok 2001).

Observations of the rotation curve of NGC 3109 suggest a dominant dark-matter halo (Jobin & Carignan 1990), which cosmological N-body cold dark matter (CDM) simulations have struggled to reproduce (Navarro et al. 1996). NGC 3109 has also lent itself to tests of the predictions of modified Newtonian dynamics (MOND; Milgrom 1983), but observational uncertainties such as the adopted distance led to differing conclusions (Lake 1989; Milgrom 1991). Improved observational data (e.g., Blais-Ouellette et al. 2001) have helped the situation, but the debate continues (e.g., Valenzuela et al. 2007 and references therein).

As part of the larger ARAUCARIA project (PI: Gieren), we have obtained spectroscopy of some of the most visually luminous stars in NGC 3109, using the Very Large Telescope (VLT) of the European Southern Observatory (ESO). These are the first spectroscopic observations of resolved stars in this galaxy, enabling us to study the kinematics and abundances of the young stellar population in this dark-matter–dominated dwarf. The observations are detailed in § 2, followed by classification of the spectra in § 3. Stellar radial velocities are presented in § 4, in which we have compared them with H I rotation curves, and in § 5 we undertake a quantitative analysis of eight stars to investigate their chemical abundances. Lastly, in § 6 we suggest NGC 3109 as a target for future large telescopes.

2. TARGET SELECTION AND OBSERVATIONS

The data were taken with the FORS2 (focal-reducer, low-dispersion spectrograph) instrument at the VLT on 2004 February 24 and 25. The multiobject spectroscopy with moveable slits (MOS) mode of operation was used with the 600B grism for the blue-region observations and the 1200R grism in the red. Targets were selected from V- and I-band photometry obtained as part of the ongoing Cepheid variable search program at the Las Campanas Polish 1.3 m telescope (Pietrzyński et al. 2006). In conjunction with new J- and K-band VLT observations, these data have been used to obtain a distance to NGC 3109 of 1.30 ± 0.02 Mpc (Soszyński et al. 2006), the most precise distance estimate to date.

Figure 1 shows the location of our targets in the color-magnitude diagram. Secondary targets were also observed serendipitously in some slitlets; the spectra of these were also extracted when we reduced the data. This is the origin of the redder targets in Figure 1, in particular the G-type supergiant with $(V - I) \sim 1.7$.

Finding charts from the FORS V-band preimaging are given in Figures 2, 3, and 4. For reference, the three strongly saturated stars in Figure 2 are those near the "F2" label in Figure 1 from Bresolin et al. (1993). Moving eastward from the three reference stars, the FORS fields roughly span the F2, F1, D2, and D1 fields from Bresolin et al. Note the slight "drift" northeastward in the astrometry for the targets in the western part of Figure 3. These were selected from a different FORS preimage, but the offset of the target stars is evident from the isolated bright targets. Stars 4, 45, and 61 were secondary targets that happened to be in the CCD gap in the preimage. Our fields also overlap with the imaging from Greggio et al. (1993). The western quarter of Figure 2 is in their region C, and nearly all of our targets shown in Figure 3 are encompassed by their region A.

[2] UK Astronomy Technology Centre, Royal Observatory, Blackford Hill, Edinburgh, UK.

[3] Institute for Astronomy, Honolulu, HI.

[4] Universidad de Concepción, Departamento de Fisica, Astronomy Group, Concepción, Chile.

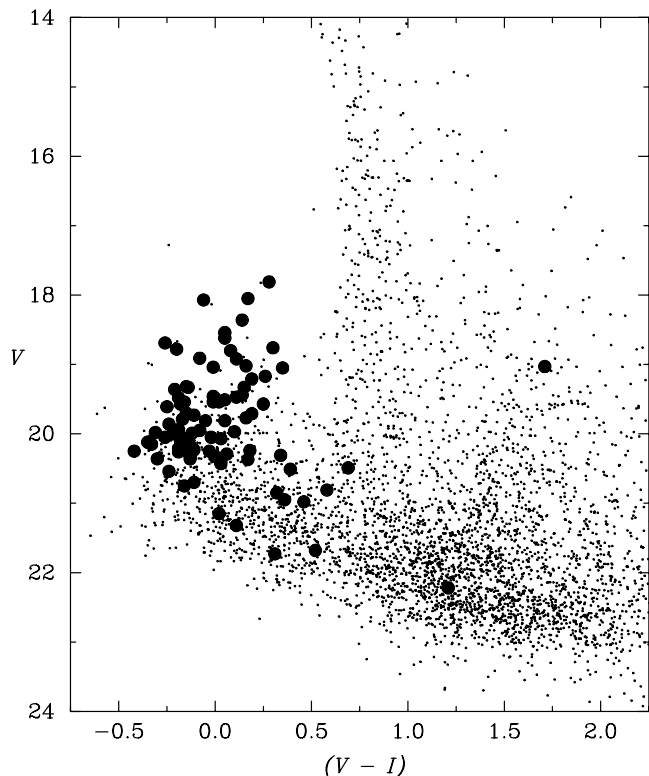[5] Warsaw University Observatory, Warsaw, Poland.

Fig. 1.—Color-magnitude diagram of VLT-FORS targets in NGC 3109 (*large closed circles*), selected from *V*- and *I*-band photometry (Pietrzyński et al. 2006).

Prior to extraction of the spectra, the L.A.COSMIC routines from van Dokkum (2001) were used to clean the frames of cosmic rays. The spectra were then bias corrected, extracted, and wavelength calibrated using IRAF (ver. 2.12).[6] An optimal extraction was used for the blue spectra, but we employed a simpler summed extraction routine for the red data—we prefer this method as nebular and/or intrinsic emission at Hα can sometimes lead to problems with sky subtraction when using optimal extractions. Indeed, accurate sky subtraction is still challenging in those stars with strong, nearby nebula emission. Further manipulation of the spectra was done with the Starlink package DIPSO, including correction to the heliocentric frame and rectification.

The observations are summarized in Table 1. In Table 2 we list the observational details for each star, by column these are (1) running identifier; (2) FORS field of observation; (3) right ascension; (4) declination; (5) V magnitude; (6) $V - I_C$ color; (7) spectral type; (8) radial velocity in km s^{-1}; (9) 1 σ uncertainty of radial velocity; (10) number of absorption lines measured in determination of the radial velocity; (11) signal-to-noise ratio of the spectrum near to Hγ; and (12) additional comments such as cross-identifications with other catalogs (e.g., Sandage & Carlson 1988), or presence of strong nebular emission lines.

The FWHM resolution (as defined by the arc lines) for the 600B data is approximately 4.6 Å, corresponding to 3.2 pixels. For the 1200R spectra this is 6.1 Å (3.1 pixels). These both give a spectral resolving power R of $\sim$1000. As a consequence of the MOS slitlets the exact wavelength coverage varies, but the $\lambda\lambda$3650–5550 region is covered by all of the blue spectra.

2.1. *Photometric Variability*

The photometry from Pietrzyński et al. (2006) was primarily obtained to monitor Cepheid variables, so we have 70–80 photometric observations of each of our stars. The data were acquired over two seasons, with three-quarters of them from the first season (spanning Julian Dates 2,452,343 to 2,452,359).

The V magnitudes and $V - I_C$ colors in Table 2 are the means of the multiepoch values. The expected scatter of the photometric results at a given magnitude is illustrated by Figure 2 from Pietrzyński et al. (2006), in which their photometry is compared to that from S. Hidalgo et al. (2007, in preparation). At $V \sim 18$ there is excellent agreement, with an increasing scatter toward fainter magnitudes (of order ± 0.1 mag at $V = 20$).

We find evidence for variability (>0.1 mag) in 5 of our targets that are brighter than $V = 20$, as shown in Figure 5. To give an indication of the scatter of the individual measurements, the light curve of a nonvariable star (No. 7) is also shown. There may be small-scale periodic (or aperiodic) variations in our other targets that are undetected from qualitative inspection, but these are not explored further here.

3. SPECTRAL CLASSIFICATION

With previous studies suggesting that the metallicity of NGC 3109 is comparable to that of the SMC (e.g., Elias & Frogel 1985), the FORS spectra were classified by comparison to published SMC spectra. For B-type supergiants we use the SMC standards published by Lennon (1997) and for A- and later-type stars we use the criteria from Evans & Howarth (2003) and Evans et al. (2004). These sources have already tackled the issue of classification at low metallicities in the MK system. For O-type spectra we rely on the digital atlas of Walborn & Fitzpatrick (1990), with reference to the SMC data presented by Walborn et al. (2000).

In addition to the low foreground reddening, the total line-of-sight reddening is also relatively low for stars in the major axis of NGC 3109, with $E(B - V) \sim 0.14$ (Davidge 1993). From the O star spectra shown in Figure 6 it can be seen that there is some contamination of the spectra by interstellar Ca K and H (at λ3933 and λ3968, respectively, with the latter blended with Hϵ at λ3970). The intensity of the interstellar components are comparable to those seen in some SMC spectra (compare with the O-type spectra shown in Figure 2 from Evans et al. 2004), and should not strongly affect the classifications for the A-type spectra— particularly as the intensity of the metallic absorption lines is also considered when classifying.

The resolution from FORS ($\sim$4.5 Å in the blue) is lower than that usually used for precise classification. We have taken this into account when classifying the spectra (largely by degrading the standards to the same effective resolution). Classifications for our targets are given in Table 2.

For spectra with signal-to-noise ratios of greater than 50, we show the blue-region data ($\lambda\lambda$3900–4750) in Figures 6–12. To highlight the spectral sequence more clearly, there is deliberate repetition of some spectra.

3.1. *Comments on Individual Stars*

We now give further explanation of our adopted spectral types for some of the targets that display peculiar or interesting features, nonunique types, etc.

Star 2 (*mid-Be; Fig. 10*).—There is significant emission in the Balmer series in this spectrum. The intensities of the He I and Mg II lines are consistent with a mid B-type classification (of $\sim$B3-5), although of course there may be in-filling in the helium lines
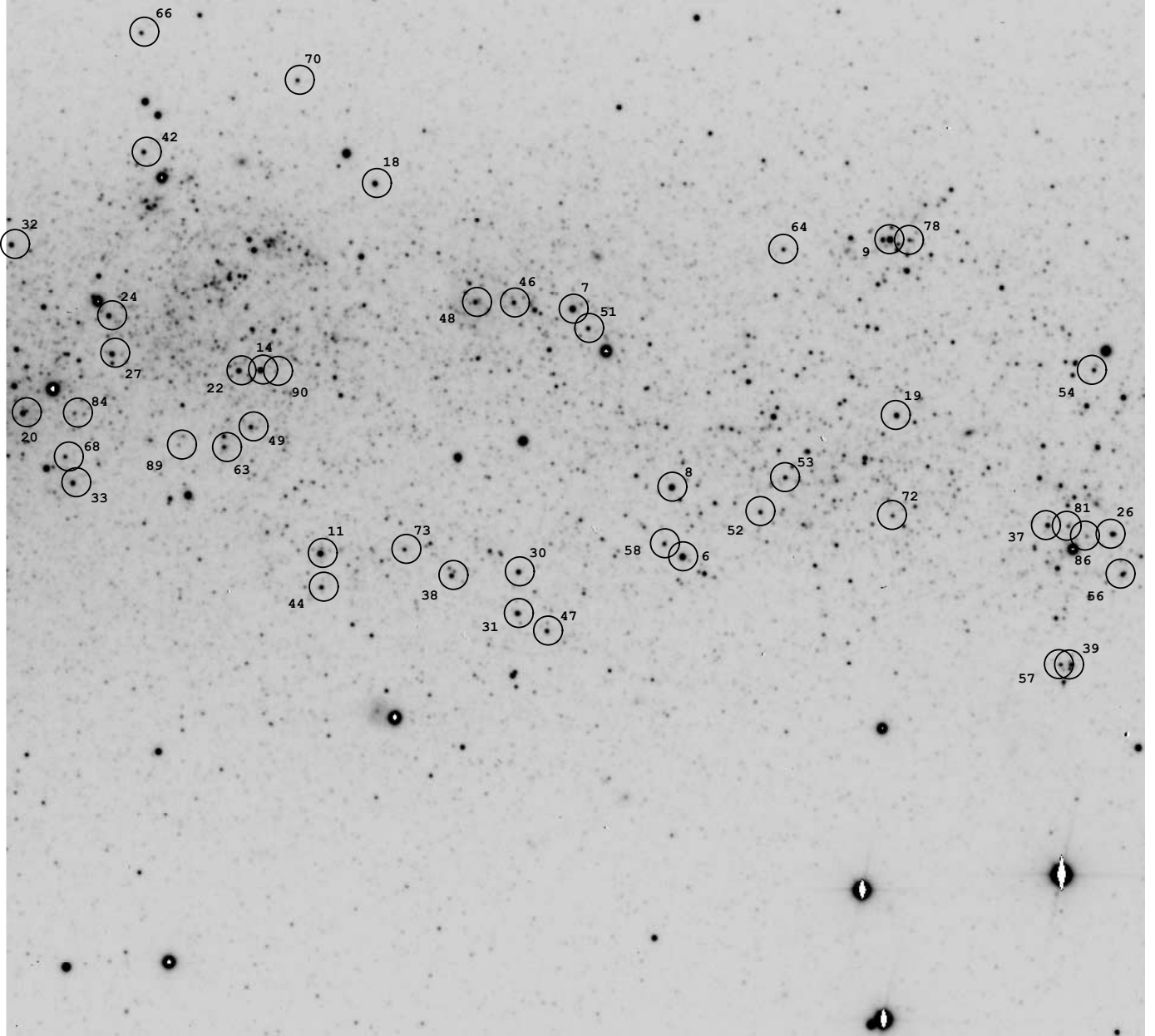
FIG. 2.—FORS *V*-band preimaging of NGC 3109, with our spectroscopic targets encircled. North is at the top, and east to the left. For reference the three saturated stars at the southwest of the frame are those just south of the "F2" label in Fig. 1 of Bresolin et al. (1993). The image is roughly 4.0′ squared.
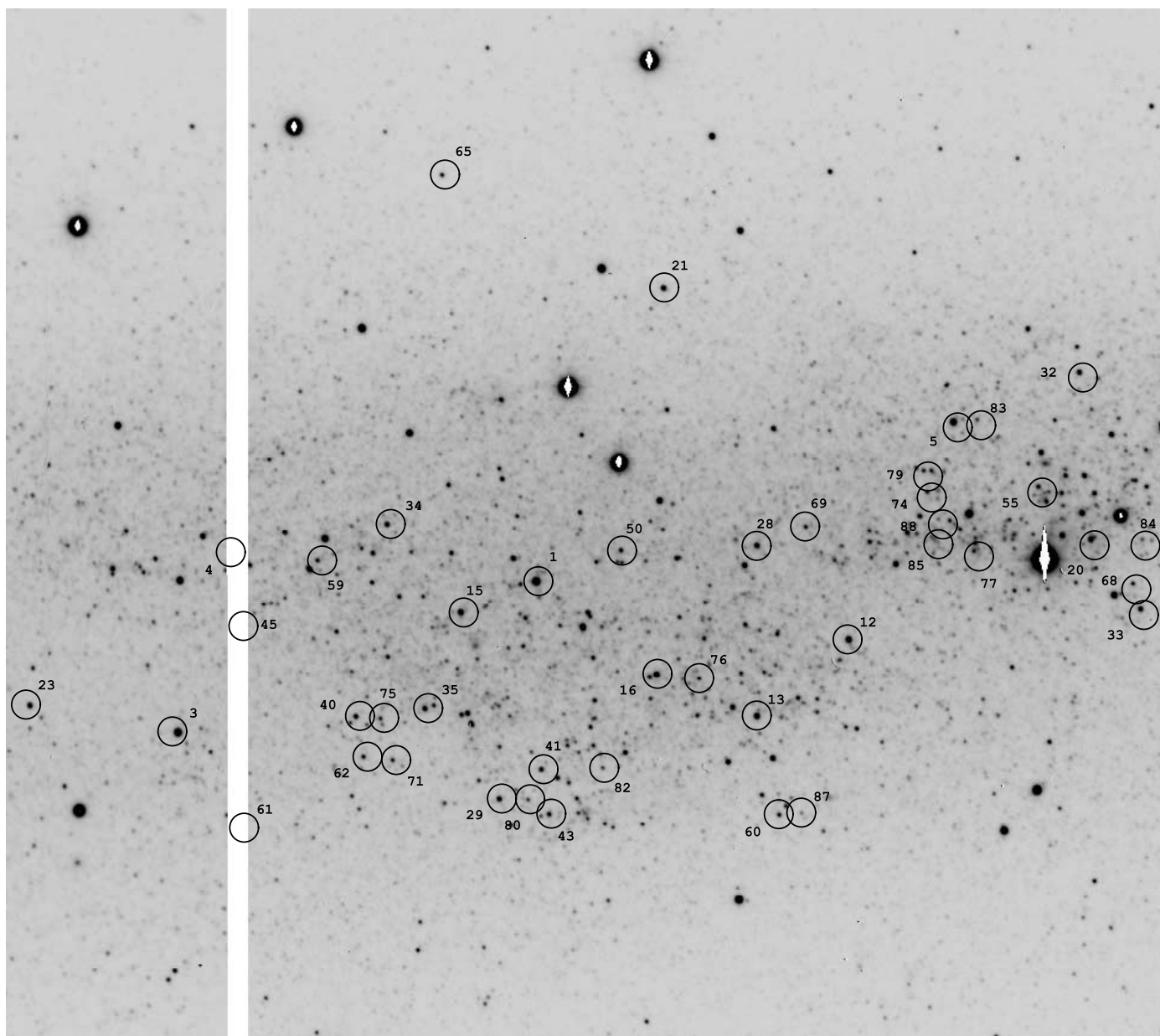
F<small>IG</small>. 3.—Target stars in NGC 3109, moving eastward from Fig. 2.
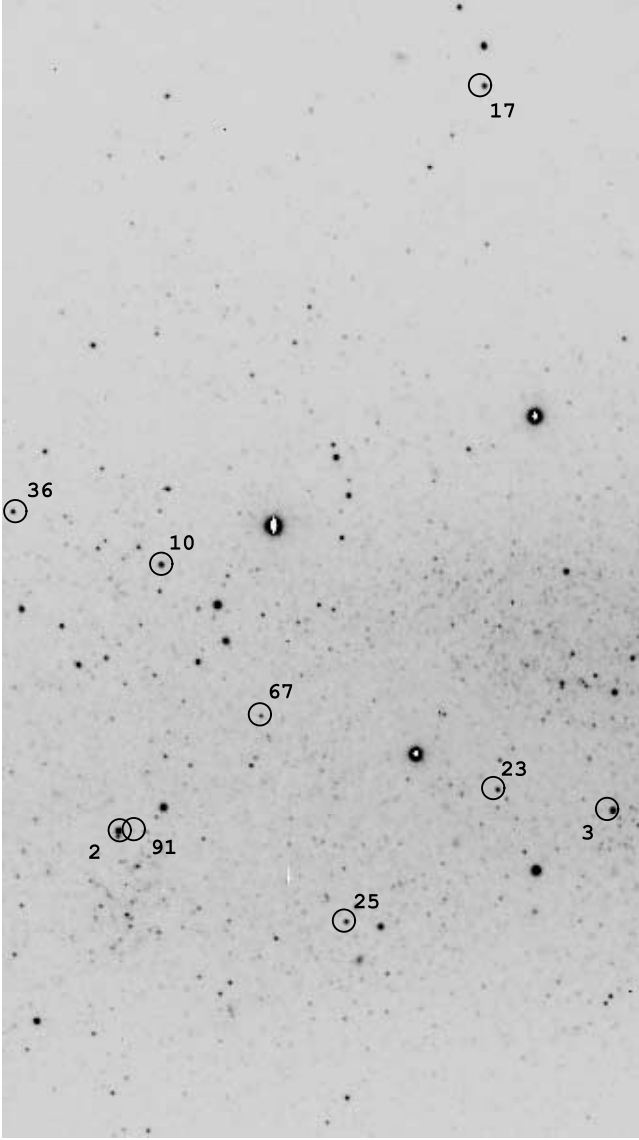
Fig. 4.—Target stars in NGC 3109, moving eastward from Fig. 3. To include star 17 the image shown here is approximately $3.0' \times 5.0'$.

TABLE 1
SUMMARY OF OBSERVATIONS

Field	Grism	Date	Exposure Time (s)
1......................	600B	2004 Feb 24	4×2700
2......................	600B	2004 Feb 25	4×2400
3......................	600B	2004 Feb 24	$3 \times 2700 + 1 \times 2400$
4......................	600B	2004 Feb 25	$1 \times 2700 + 2 \times 2400$
1......................	1200R	2004 Feb 24	4×2500
2......................	1200R	2004 Feb 25	4×2400

Star 24 (B2-3 Iab; Fig. 9).—The absence of Si III combined with Mg II absorption (albeit weak) requires a type of B3. However, there is also weak absorption from O II $\lambda 4650$ that would not usually be expected, suggesting a slightly earlier type.

Star 35 [O8–9.5 I(f); Fig. 6].—The strength of the He II $\lambda 4542$ absorption is consistent with an earlier type than the $\lambda 4200$ line, leading to a range of possible classifications for this spectrum. Weak N III emission is seen at $\lambda\lambda 4634, 4640, 4642$, with in-filled He II $\lambda 4686$.

Star 36 (mid-B; Fig. 10).—P Cygni emission is seen in both the Hγ and Hβ lines; similarly at Hα (Fig. 13). The ratio of Si II $\lambda\lambda 4128–4132$ to He I $\lambda 4121$ requires a mid to late B-type classification for this spectrum, well matched by the other He I lines. However, the weakness of the Mg II $\lambda 4481$ feature contradicts this somewhat, suggesting a slightly earlier type.

Star 59 (B0-3; Fig. 9).—Weak absorption is seen from Si III, but a precise spectral type cannot be assigned due to the absence of other diagnostic lines (such as Mg II $\lambda 4481$, the CNO blend at $\sim\lambda 4650$, etc.).

Star 91 (B1-2e [shell]; Fig. 9).—The Balmer lines in this spectrum are very narrow, resembling those seen in shell stars. The presence the $\lambda 4650$ blend suggests an early B-type, but we lack other diagnostic lines to assign a unique type (e.g., Si III, Si IV, Mg II). With moderate signal-to-noise observations of low-metallicity targets, this is a common problem in this spectral domain (e.g., star 59 above, and Evans et al. 2004). This star appears to be heavily reddened, although it is at the faint end of the photometric survey and so a relatively large degree of uncertainty in the color can probably be expected (see Pietrzyński et al. 2006).

4. STELLAR RADIAL VELOCITIES

Radial velocities, v_r, were calculated from the means of manual measurements of the line centers of absorption lines. Where possible the primary Balmer lines (Hβ, Hγ, Hδ, H8, and H9) were supplemented by measurements of He I and He II lines, and occasionally from metallic lines (e.g., in the luminous B-type supergiants). We do not use the Hϵ line owing to its blend with the Ca H line.

The mean v_r values for each of our targets are given in Table 2, together with 1 σ uncertainties and the number of lines used (dependent on both the spectral type of the star, and the data quality). To investigate the spatial variation of the radial velocities we initially binned our results. The median 1 σ (internal) uncertainty is 19 km s^{-1}, but we adopt a more conservative bin size of 50 km s^{-1} (thereby also providing a reasonable number of stars per bin). In Figure 14 we show the spatial distribution of the stars in each of four bins, i.e., $v_r < 350$, $350 < v_r < 400$, $400 < v_r < 450$, and $v_r > 450$ km s^{-1}. Although limited by both sample size and velocity precision, Figure 14 shows a trend of increasing velocities

and/or continuum effects from a circumstellar disk. There is weak [N II] emission in the wings of the Hα profile (see Fig. 13), but the scale and extent of the Hα emission suggests a primarily nonnebular origin, hence the Be-type classification.

Star 7 (B0-1 Ia; Fig. 7).—The uncertainty in this spectral type arises from what appears to be very weak He II $\lambda 4542$. The spectrum is otherwise consistent with that of a B1-type supergiant.

Star 9 (B0.5 Ia; Fig. 7).—This bright star has a nearby companion (see Fig. 2) to the extent that the spatial profiles were somewhat blended prior to extraction. The dominant spectrum appears to be that of a B0.5 supergiant, with weak He II $\lambda 4686$ absorption.

Star 12 (B8 Ia; Fig. 10).—The blue spectrum of star 12 shows increasing amounts of in-filling in Balmer lines as one moves redward, presumably from a stellar outflow. The Hα profile displays broad and strong emission (with an equivalent width of 7.5 ± 0.3 Å).

Star 22 (B1 Ia; Figs. 7 and 8).—From qualitative inspection the N II $\lambda 3995$ line in this spectrum appears relatively strong for its type (but see comment in § 5).

TABLE 2

Observational Parameters of Target Stars

Star (1)	Field (2)	α (J2000.0) (3)	δ (J2000.0) (4)	V (5)	V − I_C (6)	Spectral Type (7)	v_r (km s^{-1}) (8)	σ (km s^{-1}) (9)	No. of Lines (10)	S/N (11)	Comment (12)
1....................	2	10 03 11.93	−26 09 29.01	17.81	0.28	A2 Ia	412	9	5	195	
2....................	1	10 03 27.47	−26 10 06.41	18.05	0.17	Mid-Be	477	9	6	180	SC88, B155
3....................	1	10 03 17.66	−26 10 00.67	18.07	−0.06	B1 Ia	419	24	9	110	SC88, B80
4....................	2	10 03 16.74	−26 09 22.90	18.36	0.14	B9 Ia	454	25	8	100	SC88, B75
5....................	2	10 03 05.37	−26 08 56.58	18.54	0.05	B8 Ia	411	23	10	95	SC88, B56
6....................	2	10 02 52.99	−26 09 51.65	18.62	0.05	B8 Ia	370	8	10	140	SC88, B34
7....................	2	10 02 54.69	−26 08 59.64	18.69	−0.26	B0-1 Ia	382	19	10	110	SC88, B138
8....................	3	10 02 53.15	−26 09 37.03	18.76	0.30	A7 II	393	19	5	95	SC88, B36
9....................	2	10 02 49.77	−26 08 45.04	18.78	−0.20	B0.5 Ia	375	16	9	140	SC88, B136
10....................	1	10 03 26.63	−26 08 54.24	18.80	0.08	B: +em/neb?	464	20	5	65	SC88, B120
11....................	1	10 02 58.61	−26 09 50.95	18.91	−0.08	B0 I	354	22	7	125	SC88, B148
12....................	1	10 03 07.09	−26 09 41.26	18.92	0.11	B8 Ia	399	15	7	80	SC88, B57
13....................	2	10 03 08.51	−26 09 57.31	19.02	0.16	A0 Iab	405	12	5	130	SC88, B67
14....................	2	10 02 59.54	−26 09 12.44	19.03	1.71	G2 I	317	18	3	−	SC88, R14
15....................	2	10 03 13.10	−26 09 35.61	19.04	−0.01	B5 Ia	419	17	12	120	SC88, B90
16....................	2	10 03 10.06	−26 09 48.53	19.05	0.35	A7 II	381	17	5	60	
17....................	1	10 03 20.21	−26 06 44.62	19.17	0.26	A3 II	447	23	5	50	DKI 1874
18....................	2	10 02 57.76	−26 08 33.25	19.21	0.19	B1 I	392	29	6	105	SC88, B104
19....................	3	10 02 49.67	−26 09 21.95	19.32	−0.15	B1 Ia	363	17	11	85	SC88, B33
20....................	2	10 03 03.22	−26 09 21.41	19.33	−0.14	O8 I	407	11	8	70	
21....................	3	10 03 09.96	−26 08 27.11	19.33	0.15	A0 Iab	397	20	5	50	
22....................	2	10 02 59.88	−26 09 12.60	19.36	−0.21	B1 Ia	391	25	14	65	
23....................	1	10 03 19.95	−26 09 55.01	19.44	0.14	A1 Ib	453	18	5	130	SC88, V14a
24....................	1	10 03 01.89	−26 09 01.04	19.46	−0.01	B2-3 Iab	346	15	11	80	
25....................	1	10 03 22.95	−26 10 30.91	19.47	0.11	A0 Ib	429	7	5	90	
26....................	2	10 02 46.32	−26 09 46.88	19.48	−0.19	B3 Ib	337	13	11	140	
27....................	2	10 03 01.85	−26 09 08.91	19.49	0.00	B2.5 Ia	420	17	10	90	
28....................	1	10 03 08.51	−26 09 21.56	19.51	0.05	B2.5 Iab	390	30	11	90	
29....................	1	10 03 12.50	−26 10 14.81	19.54	0.02	B8 Ia	421	13	8	75	
30....................	2	10 02 55.53	−26 09 54.82	19.54	−0.01	A0 Iab	400	21	7	85	
31....................	3	10 02 55.55	−26 10 03.57	19.54	−0.16	B1-2 Ib	409	34	10	60	
32....................	1	10 03 03.41	−26 08 46.06	19.57	0.25	A3 II	370	8	5	95	SC88, V7,65a
33....................	3	10 03 02.45	−26 09 36.11	19.57	−0.18	O9 If	334	33	5	60	
34....................	1	10 03 14.24	−26 09 16.96	19.61	−0.25	O8 I(f)	409	25	10	90	
35....................	3	10 03 13.65	−26 09 55.76	19.70	−0.15	O8-9.5 I(f)	476	16	7	60	
36....................	1	10 03 29.56	−26 08 39.96	19.71	0.19	Mid-B	. . .	. . .	. . .	80	P Cyg em.
37....................	2	10 02 47.33	−26 09 45.07	19.73	−0.11	B2 Iab	364	22	13	90	
38....................	2	10 02 56.57	−26 09 55.58	19.77	0.16	B1-3 III	379	30	8	50	
39....................	4	10 02 46.97	−26 10 14.34	19.79	−0.17	O9.5 II:	337	33	6	70	
40....................	2	10 03 14.72	−26 09 57.40	19.81	−0.05	B8 Ib	430	13	5	90	
41....................	3	10 03 11.85	−26 10 08.64	19.81	0.05	A0 Iab	454	28	4	55	
42....................	3	10 03 01.36	−26 08 26.69	19.86	−0.24	B0-2	428	22	5	55	
43....................	4	10 03 11.73	−26 10 18.00	19.94	−0.19	O9.5 I	424	24	6	40	
44....................	3	10 02 58.59	−26 09 58.04	19.95	−0.08	Early-B Ib	394	33	7	35	
45....................	4	10 03 16.55	−26 09 38.46	19.97	0.10	B8-A0 I	441	20	5	25	
46....................	4	10 02 55.61	−26 08 58.35	19.98	−0.31	Early-B	394	15	9	40	
47....................	3	10 02 55.09	−26 10 07.25	19.99	−0.12	B2.5 Ib	408	28	6	65	
48....................	4	10 02 56.20	−26 08 58.23	19.99	−0.19	Late-O If	. . .	. . .	. . .	40	MRS07, H II, No. 8
49....................	3	10 02 59.69	−26 09 24.38	20.00	−0.22	O9 II	390	29	5	40	
50....................	1	10 03 10.62	−26 09 22.56	20.05	−0.02	B8: Ib	399	10	3	80	
51....................	4	10 02 54.45	−26 09 03.69	20.05	−0.26	Early-B (B0?)	351	20	5	60	
52....................	3	10 02 51.78	−26 09 42.14	20.07	0.03	A0 Ib	381	22	5	45	
53....................	4	10 02 51.40	−26 09 35.02	20.07	−0.16	B0: Ib	405	35	5	55	
54....................	3	10 02 46.61	−26 09 12.45	20.10	−0.18	B1-3 II-Ib	352	23	5	45	
55....................	4	10 03 04.04	−26 09 10.30	20.12	−0.35	B0-2	413	19	6	45	Strong H II at Hβ
56....................	4	10 02 46.16	−26 09 55.26	20.14	−0.17	Early-B	−	−	−	65	
57....................	4	10 02 47.12	−26 10 14.27	20.15	−0.33	Early-B	372	22	6	45	
58....................	4	10 02 53.27	−26 09 48.92	20.17	−0.13	B9: Iab	385	10	5	35	
59....................	1	10 03 15.31	−26 09 24.64	20.21	−0.19	B0-3	446	15	10	75	
60....................	3	10 03 08.17	−26 10 18.11	20.22	−0.17	B0-0.5	434	31	8	35	
61....................	3	10 03 16.54	−26 10 20.96	20.23	−0.11	Early-B?	. . .	. . .	. . .	60	Strong H II
62....................	3	10 03 14.60	−26 10 06.00	20.24	0.18	A5 II	475	19	5	50	SC88, V9, 45, 57a
63....................	1	10 03 00.10	−26 09 28.72	20.25	−0.42	Late-O	. . .	. . .	. . .	55	MRS07, H II, No. 14
64....................	2	10 02 51.43	−26 08 47.06	20.25	−0.03	B0-2	565	23	8	55	

TABLE 2—*Continued*

Star (1)	Field (2)	α (J2000.0) (3)	δ (J2000.0) (4)	V (5)	V − I_C (6)	Spectral Type (7)	v_r (km s^{-1}) (8)	σ (km s^{-1}) (9)	No. of Lines (10)	S/N (11)	Comment (12)
65..................	4	10 03 13.39	−26 08 03.31	20.26	−0.19	Early-B	490	16	4	35	Shell star?
66..................	4	10 03 01.39	−26 08 01.48	20.29	0.06	Late-O	...	...	...	40	Strong H II
67..................	1	10 03 24.64	−26 09 35.03	20.31	0.34	A5 II	454	11	5	50	
68..................	4	10 03 02.57	−26 09 30.70	20.33	0.00	A0 Iab:	412	15	5	30	
69..................	4	10 03 07.76	−26 09 17.48	20.36	−0.13	Early–mid-B	408	33	6	30	
70..................	4	10 02 58.97	−26 08 11.58	20.36	−0.30	B5 Ia	424	33	5	40	SC88, V6,25,31a
71..................	4	10 03 14.15	−26 10 06.71	20.37	0.17	B9-A0 Ib:	405	30	4	35	
72..................	4	10 02 49.73	−26 09 42.95	20.40	0.03	A0 Ib:	394	29	5	40	
73..................	4	10 02 57.30	−26 09 50.10	20.43	0.03	A0: Iab	392	11	5	35	
74..................	3	10 03 05.77	−26 09 11.36	20.44	...	B0-2 II:	440	17	5	40	
75..................	2	10 03 14.34	−26 09 57.82	20.49	0.69	F2 I	504	12	4	−	
76..................	4	10 03 09.41	−26 09 49.43	20.51	0.39	B9-A0 Ib	370	23	4	35	
77..................	3	10 03 05.03	−26 09 23.78	20.52	...	Late-O	...	...	...	40	MRS07, H II, No. 21
78..................	2	10 02 49.47	−26 08 45.18	20.54	−0.24	O9.5 III	402	25	9	70	
79..................	2	10 03 05.83	−26 09 06.92	20.55	...	B9 Ib	407	11	4	40	
80..................	1	10 03 12.06	−26 10 14.97	20.70	−0.11	Early-B (B1-2)	398	18	8	40	
81..................	2	10 02 47.00	−26 09 45.21	20.75	−0.16	B1: Ib	389	19	10	65	
82..................	3	10 03 10.90	−26 10 08.34	20.81	0.58	F2: I	382	13	3	...	
83..................	2	10 03 05.00	−26 08 56.13	20.85	0.32	A3 II	296	17	5	45	
84..................	2	10 03 02.43	−26 09 21.49	20.95	0.36	A5 II	393	27	5	30	
85..................	4	10 03 05.67	−26 09 21.20	20.98	0.46	Early-B	408	33	4	25	
86..................	2	10 02 46.72	−26 09 47.27	21.15	0.02	Late-B II	445	12	3	35	
87..................	3	10 03 07.81	−26 10 17.77	21.32	0.11	B	292	30	3	20	SC88, V36c
88..................	1	10 03 05.60	−26 09 17.03	21.41	...	Early–mid B	455	14	5	30	
89..................	1	10 03 00.81	−26 09 28.20	21.68	0.52	A5: II	263	22	4	20	
90..................	2	10 02 59.31	−26 09 12.72	21.73	0.31	A7 II:	482	14	3	25	
91..................	1	10 03 27.18	−26 10 06.11	22.22	1.21	B1-2e (shell)	440	18	9	55	

NOTE.—Units of right ascension are hours, minutes, and seconds, and units of declination are degrees, arcminutes, and arcseconds.

REFERENCES.— DKI = Demers et al. 1985, SC88 = Sandage & Carlson 1988, MRS07 = Peña et al. 2007b.
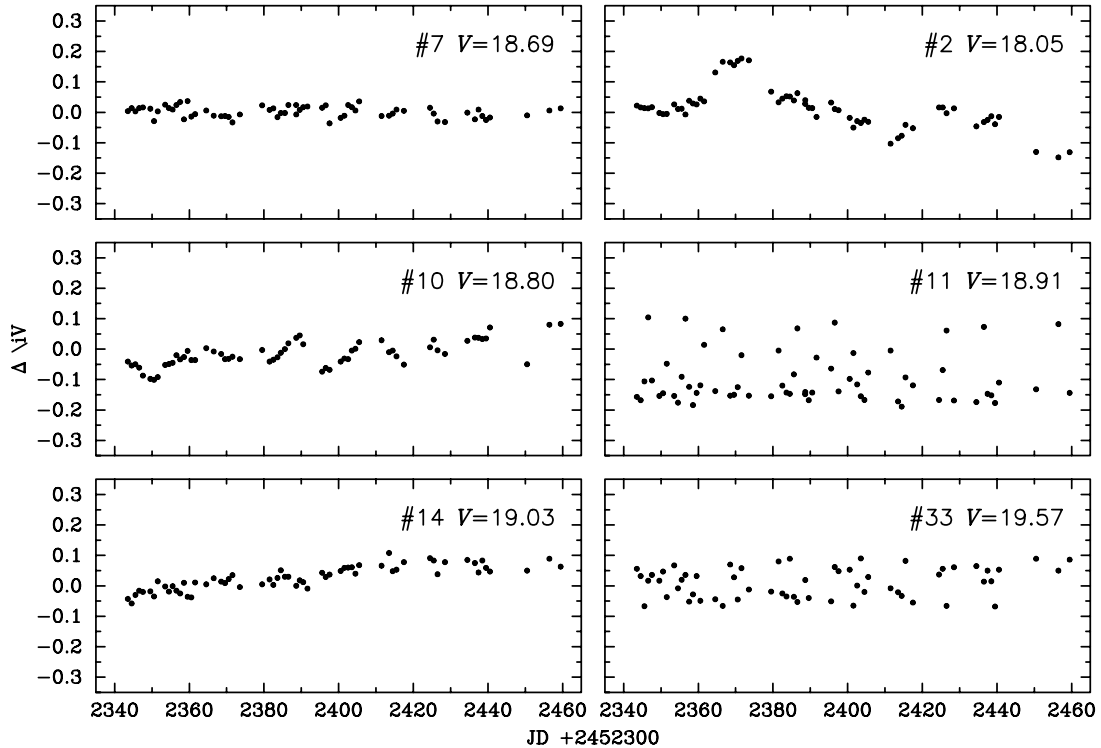

FIG. 5.—Photometric variables in NGC 3109. Star 7 is included to illustrate the scatter for a nonvariable target.
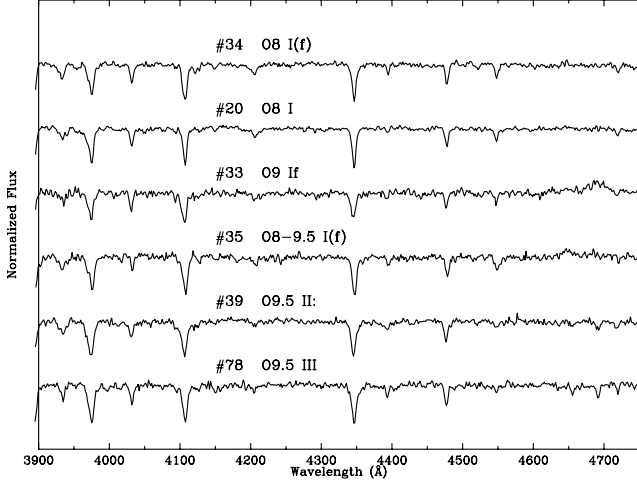
Fig. 6.—Normalized spectra of O-type stars in NGC 3109.

with increasing right ascension, i.e., rotation of the galaxy as traced by the young stellar population.

In Figure 15 we plot differential velocities, Δv (i.e., $v_r - v_{sys}$), as a function of radius along the main disk of the galaxy, taking the systemic velocity (v_{sys}) as 402 km s^{-1} (Blais-Ouellette et al. 2001). We have corrected the velocities in the figure for an inclination of 75° (Jobin & Carignan 1990). The radius is calculated by finding the radial distance of each star from the optical center of the galaxy ($\alpha = 10^h03^m06.6^s$, $\delta = -26°09'32''$ [J2000.0]; Blais-Ouellette et al. 2001), projected onto the major axis of the galaxy. The position angle of NGC 3109 is 93° (Jobin & Carignan
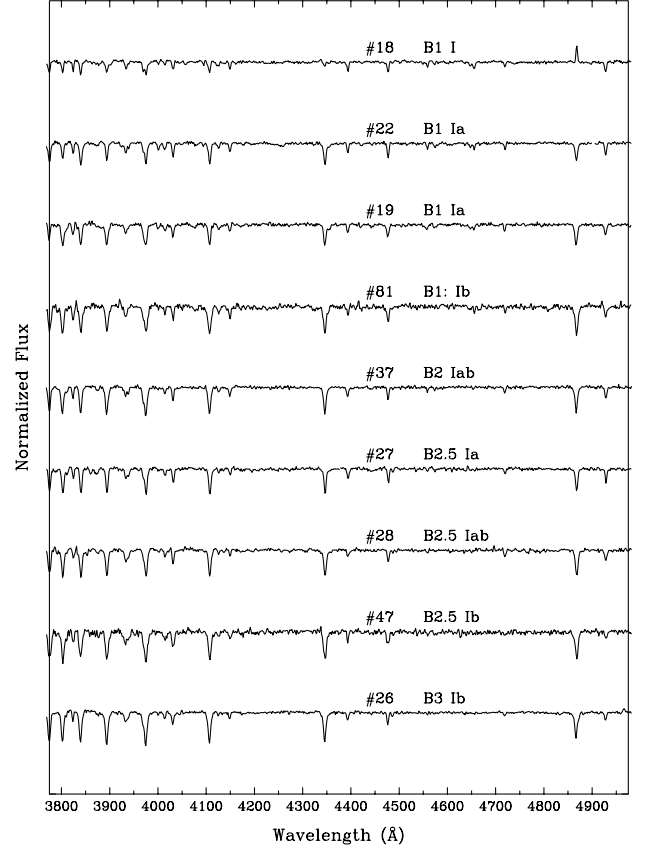

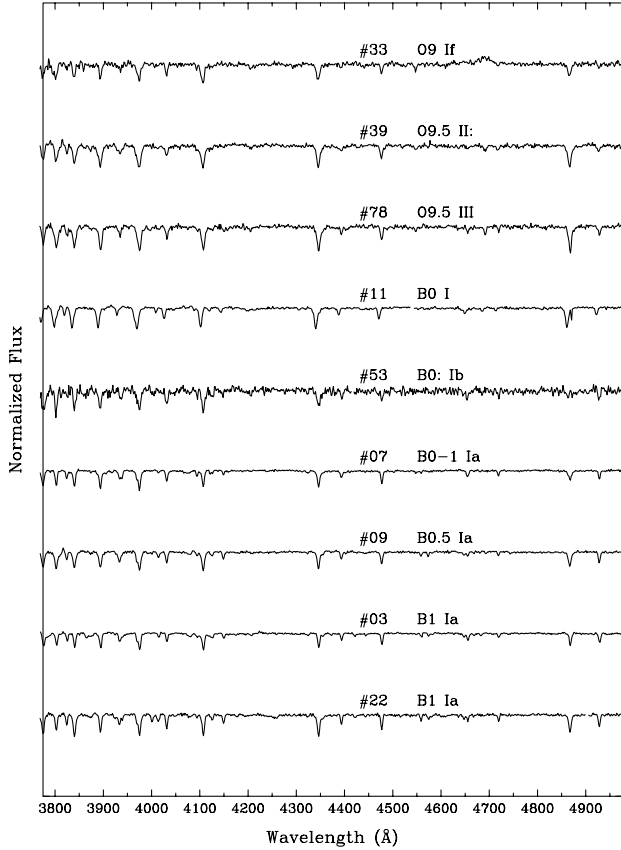Fig. 8.—Normalized spectra of early B-type supergiants.

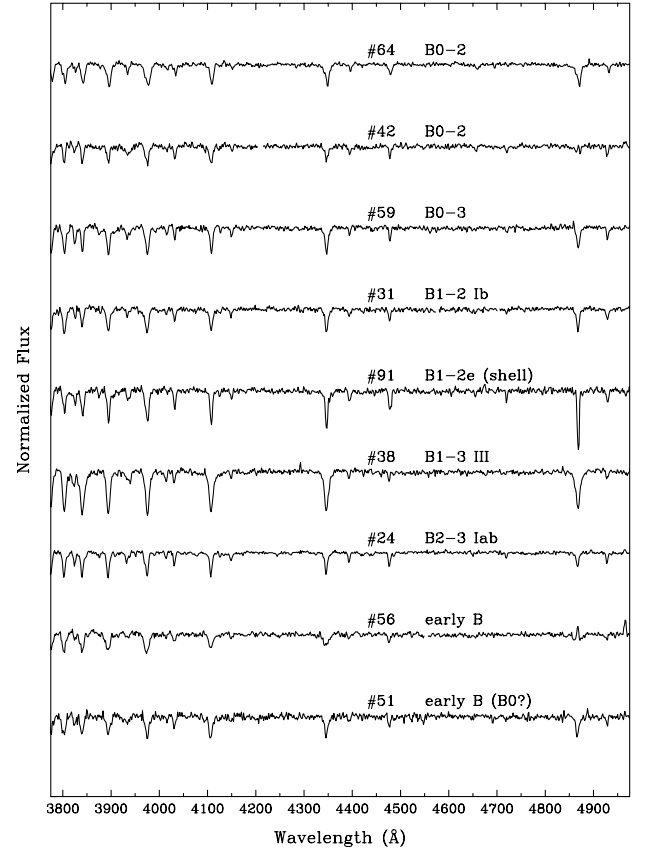Fig. 7.—Normalized spectra of stars classified in the range O9–B1.

Fig. 9.—Normalized spectra of early B-type supergiants with nonunique classifications.
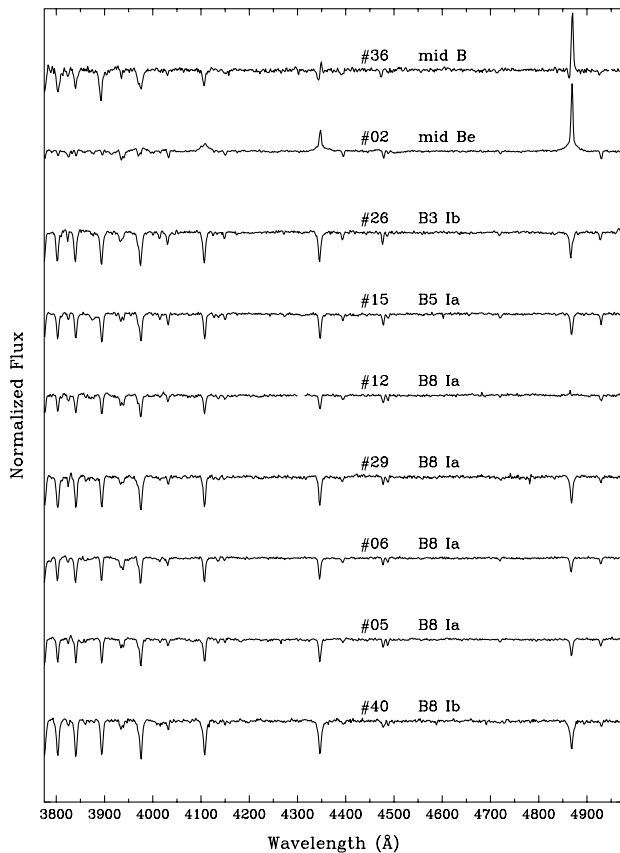
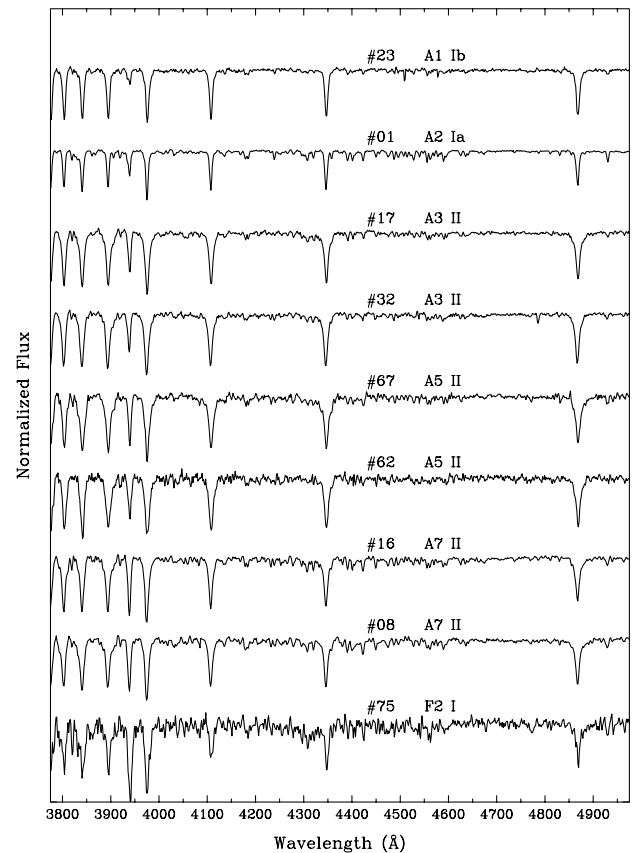FIG. 10.—Normalized spectra of mid B-type supergiants.

FIG. 12.—Normalized spectra of A-type supergiants and bright giants.

1990), so the projection term related to this component is relatively minor. In Figure 15 we also plot rotation curves from H I observations (Jobin & Carignan; *solid line*, shifted by 2 km s^{-1} so that the systemic velocities tally) and Hα (Blais-Ouellette et al.; *dotted line*).

In general, the stars track the H I and Hα rotation curves, but with a fair degree of scatter. Further observations would be of significant value to determine whether the stellar results are revealing

FIG. 13.—Hα spectra of two stars with significant emission profiles (>20 Å). The redshifted [N II] emission at $\lambda6583$ is the small "bump" redward of Hα in the spectrum of star 2.

FIG. 11.—Normalized spectra of late B- and A0-type supergiants.

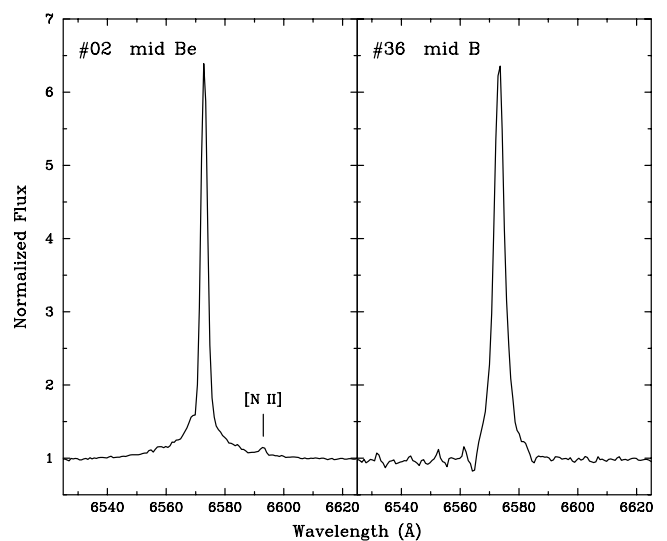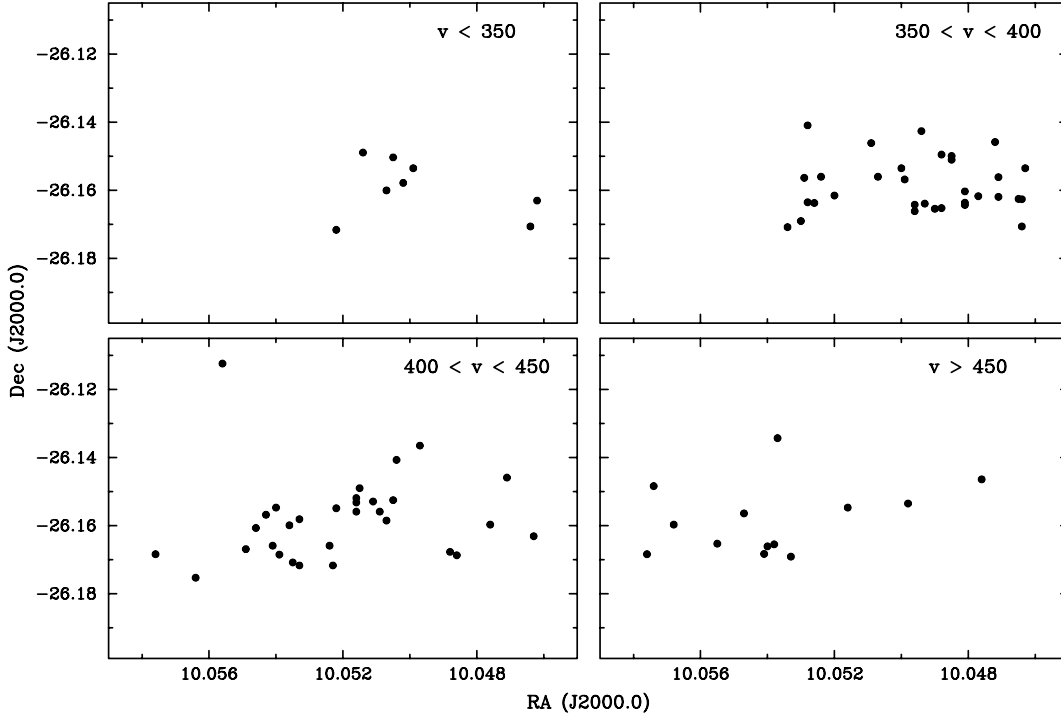Fig. 14.—Spatial distribution of NGC 3109 targets in different radial velocity bins (in km s^{-1}), indicating a velocity gradient in the kinematics of the young stellar population across the observed region.

genuine substructures in the disk, or whether we are simply limited by the small sample (and/or undetected nebular contamination at our relatively low spectral resolution).

5. STELLAR ABUNDANCES IN NGC 3109

Early B-type supergiants have numerous metallic absorption lines that are useful for abundance determinations. Here we analyze eight supergiants from our sample using the FASTWIND model atmosphere code (Santolaya-Rey et al. 1997; Puls et al. 2005). The methods for quantitative analysis at the spectral resolution from FORS are described in detail elsewhere (Urbaneja et al. 2003, 2005a). In brief, each model is described by an effective temperature ($T_{\rm eff}$), a surface gravity and a stellar radius, each of which is defined at $\tau_{\rm Ross} = 2/3$. Additional model parameters are

Fig. 15.—Stellar radial velocities, as a function of radius along the major axis of NGC 3109, corrected to the systemic velocity a 402 km s^{-1}. The median 1 σ (internal) uncertainty is 19 km s^{-1}. Also shown are rotation curves from H I (Jobin & Carignan 1990, *solid line*) and Hα (Blais-Ouellette et al. 2001, *dotted line*).

the exponent of the wind velocity law (β), the microturbulent velocity ($v_{\rm turb}$), the mass-loss rate ($\dot{M}$), the wind terminal velocity (v_∞), and a set of chemical abundances. Terminal velocities are taken from the spectral-type$-v_\infty$ relation from Kudritzki & Puls (2000).

To limit the number of free parameters, we follow the approach described by Urbaneja et al. (2005b), namely, fitting the effective temperature, surface gravity, global metallicity, and Q' (which, at fixed v_∞, takes into account the mass-loss rate and stellar radius). In calculation of the atmospheric structure $v_{\rm turb}$ is fixed to 10 km s^{-1}, but this is then varied in the spectral synthesis to obtain uniform abundances from different lines of the same metallic species.

The extinction and absolute magnitudes of our targets are given in Table 3. The color excess, $E(V - I_{\rm C})$, was calculated from the observed colors (Table 2) and intrinsic colors obtained from the FASTWIND models, convolved with the appropriate filter. Some iteration is required here, but once the stellar radius is approximately correct, the colors do not vary significantly. The V-band

TABLE 3
EXTINCTION AND ABSOLUTE MAGNITUDES FOR TARGET STARS

ID	Spectral Type	V	$V - I_{\rm C}$	$E(V - I_{\rm C})$	A_V	$E(B - V)$	M_V
11.........	B0 I	18.91	-0.08	0.16	0.41	0.13	-7.07
7...........	B0-1 Ia	18.69	-0.26	-0.04	0.27	0.09	-7.15
9...........	B0.5 Ia	18.78	-0.20	0.01	0.03	0.00	-6.82
3...........	B1 Ia	18.07	-0.06	0.10	0.26	0.08	-7.76
22.........	B1 Ia	19.36	-0.21	-0.02	0.27	0.09	-6.48
37.........	B2 Iab	19.73	-0.11	0.04	0.10	0.03	-5.94
27.........	B2.5 Ia	19.49	0.00	0.15	0.39	0.13	-6.47
28.........	B2.5 Iab	19.51	0.05	0.20	0.52	0.17	-6.58

NOTES.—The observed color excesses for stars 7 and 22 are nonphysical, due to likely contamination by nearby H II regions. The adopted $E(B - V)$ is the mean from Soszyński et al. (2006).

TABLE 4
Physical Parameters of Target Stars

ID	Spectral Type	$T_{\rm eff}$ (kK)	$\log g$	R ($R_\odot$)	$M_{\rm spec}$ ($M_\odot$)	$\log (L/L_\odot)$	$v_{\rm turb}$ (km s^{-1})	$Y_{\rm He}$	$\epsilon_{\rm N}$	$\epsilon_{\rm O}$	$\epsilon_{\rm Mg}$	$\epsilon_{\rm Si}$	[O/H] (dex)
11.................	B0 I	27.5	3.05	35.5	51.6	5.81	12	0.10	<7.3	7.8	6.9	6.7	−0.9
7...................	B0-1 Ia	27.0	2.90	37.0	39.7	5.82	12	0.10	<7.5	7.8	7.0	6.9	−0.9
9...................	B0.5 Ia	25.0	2.75	34.5	24.4	5.62	12	0.10	7.7	7.8	7.0	7.0	−0.9
3...................	B1 Ia	23.5	2.50	56.2	36.5	5.94	15	0.10	7.4	7.7	6.8	6.8	−1.0
22.................	B1 Ia	22.0	2.60	33.0	15.6	5.35	15	0.15	7.7	7.8	6.9	6.9	−0.9
37.................	B2 Iab	20.5	2.70	28.0	14.3	5.04	10	0.15	7.3	7.6	6.9	6.9	−1.1
27.................	B2.5 Ia	19.0	2.40	37.0	12.5	5.20	12	0.13	7.7	7.8	7.1	7.0	−0.9
28.................	B2.5 Iab	19.0	2.55	39.0	19.7	5.25	10	0.10	7.7	7.8	7.1	7.1	−0.9

Notes.—The value $\epsilon_{\rm X} = \log (X/H) + 12$. The ratio in the final column adopts a solar abundance of $\epsilon_{\rm O} = 8.66$ from Asplund et al. (2005).

extinction (A_V) was found using the relations from Cardelli et al. (1989) to calculate the (Cousins) I-band extinction. Absolute magnitudes (M_V) were then calculated taking the distance modulus to NGC 3109 as 25.57 (Soszyński et al. 2006). Note that nonphysical (i.e., negative) color excesses were obtained for two of our targets (stars 7 and 22), likely due to nearby H II regions. For these two stars the mean extinction from Soszyński et al. (2006) of $E(B-V) = 0.09$ was adopted.

Effective temperatures, microturbulent velocities, and silicon abundances were obtained from fits to the Si II/III/IV lines, with gravities and wind mass-loss rates obtained from fits to the Balmer lines, principally Hβ. The Hα line is a better diagnostic of the stellar wind, but at the distance of NGC 3109 the nebular emission varies on very small scales and sky subtraction becomes critical. Even with the FORS slitlets, there is evidence for over/undersubtraction in many of the Hα profiles, and we do not use Hα in our analysis. The associated uncertainties of this method are $T_{\rm eff} \pm 1000$ K and $\log g \pm 0.1$ dex (see discussion by Urbaneja et al. 2005b).

The primary abundance diagnostics for nitrogen and oxygen are N II $\lambda\lambda$3995, 5050, 5100; and O II $\lambda\lambda$4072–4076, 4317–4319, 4414–4416. There are also many weaker lines, and the optimum model is determined by attempting to reproduce as many features as possible—the results are included in Table 4. The dependence of the chemical abundances on the adopted stellar parameters is shown for two of our stars in Tables 5 and 6. The combined uncertainties from different parameters (added in quadrature) are shown in the final columns, with individual abundances robust to ± 0.2 dex.

We also estimate abundances for Mg II λ4481 and Si III $\lambda\lambda$4553–4572. These are less secure than the nitrogen and oxygen abundances due to the smaller number of lines and their relative weakness. Moreover, we do not quote carbon abundances for our stars. The primary isolated line of carbon is C II λ4267,

which is barely visible in the FORS spectra, notwithstanding the fact that there are many problems regarding the use of this line in theoretical models (e.g., Lennon et al. 2003). The rich blend of CNO lines around λ4650 can provide an indirect tracer of the carbon abundance, but from data at this spectral resolution the combined uncertainties render any value as very unreliable.

A summary of the physical parameters for the B-type supergiants is given in Table 4. The final FASTWIND models are compared with the FORS spectra in Figures 16 and 17, in which the model spectra have been smoothed to the effective resolution of the observations. In Figures 18 and 19 we show models for stars 22 and 37 in which the metallic abundances are ± 0.2 dex compared to the adopted values—in some cases individual O II lines are better fit by the increased or decreased values, but we consider the fit to multiple lines in our determination of the final abundance.

The mean oxygen abundance is $12 + \log (O/H) = 7.76 \pm 0.07$ (1 σ systematic uncertainty). This is in excellent agreement with results from H II regions. Lee et al. (2003b) give an oxygen abundance of 7.73 for one target, and Lee et al. (2003a) found a mean of 7.63 for a further five regions. Moreover, new results from ~10 compact H II regions find a mean abundance of 7.74 ± 0.10 (Peña et al. 2007a). The mean oxygen abundance found here is also comparable to recent results for stars in the WLM galaxy (Bresolin et al. 2006). We note that oxygen abundances are typically considered in 0.1 dex increments between models, so the mean values here give the impression of unrealistic precision. The median value for our eight stars is 7.8 (cf. 7.9 from the three stars in WLM). The results are significantly lower than those found for stars in the SMC, for which $\log (O/H) + 12 = 8.13$ and 8.14 for B- and A-type supergiants, respectively (Trundle et al. 2004; Trundle & Lennon 2005; Venn 1999).

Our abundance estimates for magnesium and silicon are more in keeping with those found in the SMC stars from Trundle & Lennon (2005). However, in many cases our estimates are upper

TABLE 5
Abundance Uncertainties as a Function of Stellar Parameters for Star 22

ELEMENT	Limit		$v_{\rm turb}$ (−5 km s^{-1})	ΔHe		ΔZ (+0.2 dex)	$\Delta \log Q$ (+0.2 dex)	$\sigma^{\rm c}$
	Upper[a]	Lower[b]		+0.2 dex	−0.2 dex			
N................................	−0.10	−0.01	−0.08	−0.06	−0.03	−0.06	−0.06	0.16
O................................	−0.02	−0.08	−0.08	−0.08	−0.03	−0.05	−0.05	0.16
Mg..............................	−0.09	0.00	−0.08	−0.05	−0.05	−0.05	−0.06	0.16
Si	−0.04	−0.01	−0.09	−0.07	0.03	−0.03	−0.06	0.14

[a] $T_{\rm eff} + 1000$ K; $\log g + 0.1$ dex.
[b] $T_{\rm eff} - 1000$ K; $\log g - 0.1$ dex.
[c] The global abundance uncertainty (σ) is obtained as the square root of the sum of the squares of the uncertainties.

TABLE 6
ABUNDANCE UNCERTAINTIES AS A FUNCTION OF STELLAR PARAMETERS FOR STAR 37

| ELEMENT | LIMIT | | $v_{\rm turb}$ (-5 km s^{-1}) | Δ He | | ΔZ (+0.2 dex) | $\Delta \log Q$ (+0.2 dex) | σ^c |
	Upper[a]	Lower[b]		+0.2 dex	−0.2 dex			
N..........................	−0.05	−0.08	−0.09	−0.08	−0.02	−0.05	−0.05	0.17
O..........................	0.04	−0.14	−0.09	−0.09	−0.01	−0.03	−0.05	0.20
Mg........................	−0.10	0.05	−0.11	−0.04	−0.02	−0.03	−0.03	0.16
Si.........................	0.08	−0.13	−0.13	−0.08	0.04	0.00	−0.04	0.22

[a] $T_{\rm eff}$ + 1000 K; $\log g$ + 0.1 dex.
[b] $T_{\rm eff}$ − 1000 K; $\log g$ − 0.1 dex.
[c] The global abundance uncertainty (σ) is obtained as the square root of the sum of the squares of the uncertainties.

limits, and the exact abundance of the α-elements will require higher resolution spectroscopy.

Where of note, we now provide brief comments on specific stars:

Star 11.—The O II feature at $\lambda\lambda4072-4076$ is somewhat distorted, with some uncertainty in definition of the continuum. Only upper limits are possible for both nitrogen and magnesium as there are not significant lines from either element. The mass-loss rate was fixed to reproduce Hβ, with $T_{\rm eff}$ from the ionization balance of He I/II and Si III/IV.

Star 7.—The spectrum of star 7 suffers from significant emission from a nearby H II region. Both Hα and Hβ are strongly con-

taminated, with Hγ and Hδ also in-filled somewhat. The gravity for this star was obtained from the higher order Balmer lines, which appear well reproduced. $T_{\rm eff}$ was found from the balance of He I/II and Si III/IV. Again the nitrogen abundance is an upper limit.

Star 9.—The mass-loss rate was fixed to reproduce Hβ, although the line core is not well matched—Hα shows some nebular contamination, it is likely that Hβ is also in-filled slightly.

Star 22.—The strong absorption close to $\lambda3995$ is not consistent with being from N II when the other nitrogen features in this spectrum are considered. The observed absorption is also very slightly redshifted, and its origins remain unclear.

FIG. 16.—FORS spectra ($\lambda\lambda3850-4450$) of B-type supergiants in NGC 3109 (*solid lines*) compared with the adopted FASTWIND models (*dotted lines*). In addition to the Balmer lines, the He I $\lambda\lambda4009, 4026, 4121, 4143,$ and 4388 lines are marked. Most of the absorption $\sim\lambda3933$ Å arises from the interstellar Ca K line.

FIG. 17.—FORS spectra ($\lambda\lambda4450$-5050 Å) of B-type supergiants in NGC 3109 (*solid lines*) compared with the adopted FASTWIND models (*dotted lines*). The identified absorption lines in the spectrum of star 28 are He I $\lambda\lambda4471, 4713, 4922,$ and Hβ; those of star 27 are Mg II $\lambda4481$, Si III $\lambda\lambda4553-4567$; those of star 22 are O II $\lambda\lambda4640-4650$; and that of star 11 is He II $\lambda4686$.
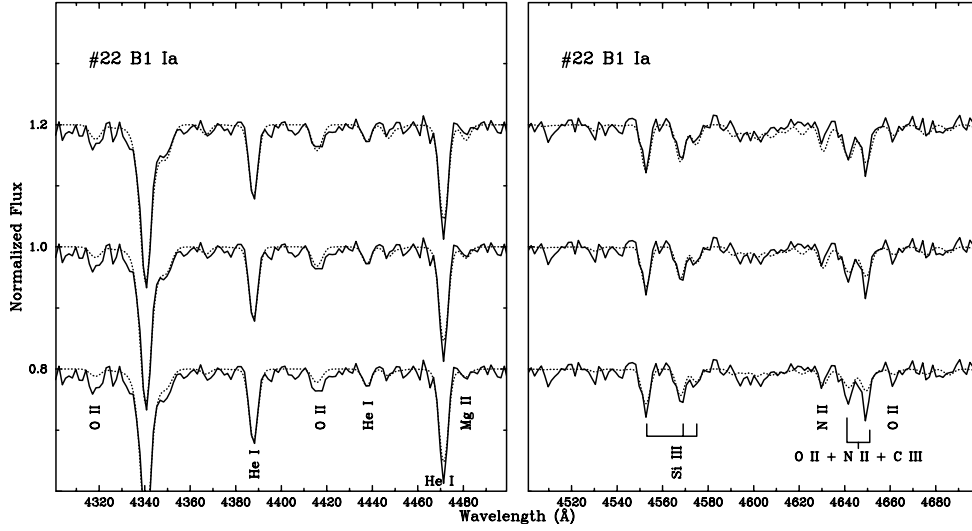
FIG. 18.—Comparison of FORS spectrum of star 22 (*solid lines*) with FASTWIND models in which the metallic abundances are ±0.2 dex compared to the adopted values (*top and bottom spectra, respectively*). The identified lines are O II λλ4317–4319, 4415–4417, 4661; He I λλ4388, 4438, 4471; Mg II λ4481; Si λλ4552, 4568, 4575; N II λ4631; and the O II + N II + C III blend at λ4650.

Star 37.—The ionization balance of Si II/III/IV is used to find T_{eff}. Note that this star is a "transitional" type in which neither the Si II nor the Si IV lines are strong.

6. NGC 3109 AS A TARGET FOR FUTURE EXTREMELY LARGE TELESCOPES

Plans for the next generation of large ground-based telescopes (the so-called extremely large telescopes [ELTs]) are now gaining momentum. Excluding the big spiral galaxies, the total stellar mass in NGC 3109 is larger than in other Local Group systems—in the context of ELTs, NGC 3109 presents an exciting opportunity to study many stages of stellar evolution in a very metal-poor environment. With a 30 m primary aperture, good signal-to-noise spectra could be obtained down to approximately $M_V = -2$. Such observations would enable detailed studies of the young, massive population (i.e., O- and early B-type stars on the main-sequence) and of stars on the asymptotic giant branch. The fainter stars could be observed at spectral resolutions comparable to those

from FORS, with higher resolutions ($R \sim 20,000$) employed to investigate wind parameters and abundances in, for example, main-sequence O-type stars.

Moreover, with less demanding signal-to-noise requirements, an ELT would be able to trace the kinematics of the less luminous population (via e.g., the calcium triplet). Crucial input to cosmological simulations could be obtained from observations along the major and minor axes of NGC 3109, to fully investigate the structure of this dark-matter–dominated dwarf.

We also note that most of the current plans for ELT instruments include some degree of adaptive optics (AO) correction (e.g., Cunningham et al. 2006). For observations in NGC 3109, a "seeing-limited" optical instrument should be adequate, e.g., the Wide Field Optical Spectrograph (WFOS) proposed for the Thirty Meter Telescope (TMT) project (e.g., Pazder et al. 2006). However, at larger distances and finer spatial scales, the AO systems will most likely restrict observers to near-IR wavelengths. Quantitative studies of OB-type stars in this domain have advanced
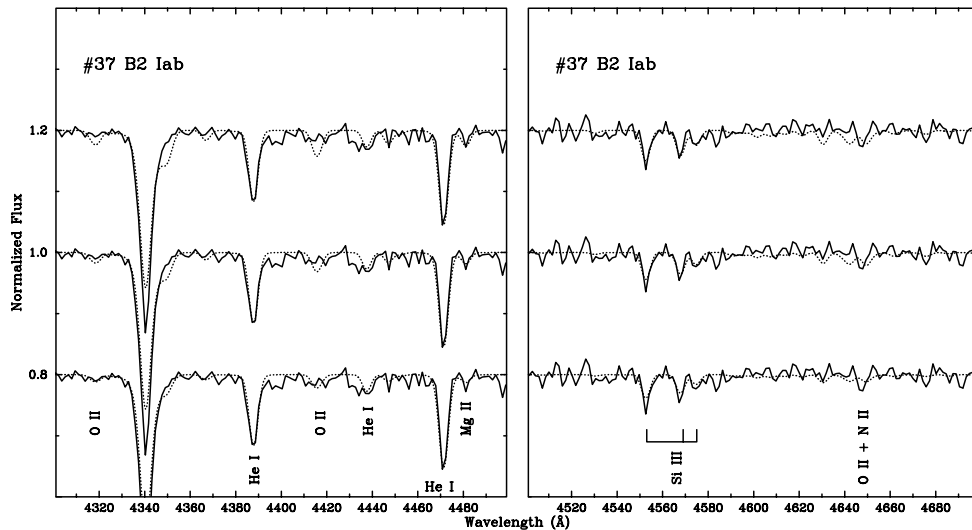

FIG. 19.—Comparison of FORS spectrum of star 37 (*solid lines*) with FASTWIND models in which the metallic abundances are ±0.2 dex compared to the adopted values (*top and bottom spectra, respectively*).

in recent years (e.g., Lenorzer et al. 2004; Repolust et al. 2005; Hanson et al. 2005). To fully exploit the likely capabilities of an ELT, continued efforts are required in this region—both in terms of atomic data (e.g., Przybilla 2005), and comparison studies in the Milky Way and Magellanic Clouds.

7. SUMMARY

We have presented spectra from an exploratory survey of the young, massive-star content of NGC 3109. These are the first spectral observations of the young stellar population in this galaxy. Although of limited resolving power, the spectra have been used to estimate stellar radial velocities, which appear largely consistent with published rotation curves from observations of the gas. Our stellar oxygen abundances agree with recent results from H II regions and are significantly lower than those found for stars in the SMC (e.g., Trundle & Lennon 2005). They are also comparable to those in the WLM galaxy (Bresolin et al. 2006). We require higher resolution spectroscopy to obtain precise abundances for the alpha-elements, but it is clear that the stars in NGC 3109 have metal abundances that are very deficient when compared to the solar neighborhood, and likely even lower than in the SMC.

REFERENCES

Asplund, M., Grevesse, N., & Sauval, A. J. 2005, in ASP Conf. Serl. 336, Cosmic Abundances as Records of Stellar Evolution and Nucleosynthesis, ed. T. G. Barnes, III & F. N. Bash (San Francisco: ASP), 25
Barnes, D. G., & de Blok, W. J. G. 2001, AJ, 122, 825
Blais-Ouellette, S., Amram, P., & Carignan, C. 2001, AJ, 121, 1952
Bresolin, F., Capaccioli, M., & Piotto, G. 1993, AJ, 105, 1779
Bresolin, F., Pietrzyński, G., Urbaneja, M. A., Gieren, W., Kudritzki, R.-P., & Venn, K. A. 2006, ApJ, 648, 1007
Burstein, D., & Heiles, C. 1984, ApJS, 54, 33
Capaccioli, M., Piotto, G., & Bresolin, F. 1992, AJ, 103, 1151
Cardelli, J. A., Clayton, G. C., & Mathis, J. S. 1989, ApJ, 345, 245
Cunningham, C., et al. 2006, Proc. SPIE, 6269, 58
Davidge, T. J. 1993, AJ, 105, 1392
de Vaucouleurs, G., de Vaucouleurs, A., Corwin, H. G., Jr., Buta, R. J., Paturel, G., & Fouqué, P. 1991, Third Reference Catalogue of Bright Galaxies (New York: Springer)
Demers, S., Battinelli, P., & Letarte, B. 2003, A&A, 410, 795
Demers, S., Kunkel, W. E., & Irwin, M. J. 1985, AJ, 90, 1967
Elias, J. H., & Frogel, J. A. 1985, ApJ, 289, 141
Evans, C. J., & Howarth, I. D. 2003, MNRAS, 345, 1223
Evans, C. J., Howarth, I. D., Irwin, M. J., Burnley, A. W., & Harries, T. J. 2004, MNRAS, 353, 601
Greggio, L., Marconi, G., Tosi, M., & Focardi, P. 1993, AJ, 105, 894
Hanson, M. M., Kudritzki, R.-P., Kenworthy, M. A., Puls, J., & Tokunaga, A. T. 2005, ApJS, 161, 154
Jobin, M., & Carignan, C. 1990, AJ, 100, 648
Kudritzki, R.-P., & Puls, J. 2000, ARA&A, 38, 613
Lake, G. 1989, ApJ, 345, L17
Lee, H., Grebel, E. K., & Hodge, P. W. 2003a, A&A, 401, 141
Lee, H., McCall, M. L., Kingsburgh, R. L., Ross, R., & Stevenson, C. C. 2003b, AJ, 125, 146
Lee, M. G. 1993, ApJ, 408, 409
Lennon, D. J. 1997, A&A, 317, 871
Lennon, D. J., Dufton, P. L., & Crowley, C. 2003, A&A, 398, 455

Lenorzer, A., Mokiem, M. R., de Koter, A., & Puls, J. 2004, A&A, 422, 275
Milgrom, M. 1983, ApJ, 270, 365
———. 1991, ApJ, 367, 490
Minniti, D., Zijlstra, A. A., & Alonso, M. V. 1999, AJ, 117, 881
Navarro, J. F., Frenk, C. S., & White, S. D. M. 1996, ApJ, 462, 563
Pazder, J., Fletcher, M., & Morbey, C. 2006, Proc, SPIE, 6269, 97
Peña, M., Richer, M. G., & Stasinska, G. 2007a, Rev. Mex. AA Conf. Ser., in press
———. 2007b, A&A, in press (astro-ph/0612553)
Pietrzyński, G., et al. 2006, ApJ, 648, 366
Przybilla, N. 2005, A&A, 443, 293
Puls, J., Urbaneja, M. A., Venero, R., Repolust, T., Springmann, U., Jokuthy, A., & Mokiem, M. R. 2005, A&A, 435, 669
Repolust, T., Puls, J., Hanson, M. M., Kudritzki, R.-P., & Mokiem, M. R. 2005, A&A, 440, 261
Sandage, A., & Carlson, G. 1988, AJ, 96, 1599
Santolaya-Rey, A. E., Puls, J., & Herrero, A. 1997, A&A, 323, 488
Soszyński, I., Gieren, W., Pietrzyński, G., Bresolin, F., Kudritzki, R.-P., & Storm, J. 2006, ApJ, 648, 375
Trundle, C., & Lennon, D. J. 2005, A&A, 434, 677
Trundle, C., Lennon, D. J., Puls, J., & Dufton, P. L. 2004, A&A, 417, 217
Urbaneja, M. A., Herrero, A., Bresolin, F., Kudritzki, R.-P., Gieren, W., & Puls, J. 2003, ApJ, 584, L73
Urbaneja, M. A., et al. 2005a, ApJ, 622, 862
———. 2005b, ApJ, 635, 311
Valenzuela, O., Rhee, G., Klypin, A., Governato, F., Stinson, G., Quinn, T., & Wadsley, J. 2007, ApJ, 657, 773
van Dokkum, P. G. 2001, PASP, 113, 1420
Venn, K. A. 1999, ApJ, 518, 405
Walborn, N. R., & Fitzpatrick, E. L. 1990, PASP, 102, 379
Walborn, N. R., Lennon, D. J., Heap, S. R., Lindler, D. J., Smith, L. J., Evans, C. J., & Parker, J. W. 2000, PASP, 112, 1243